Surface & Coatings Technology 268 (2015) 293–297

Contents lists available at ScienceDirect

Surface & Coatings Technology

journal homepage: www.elsevier.com/locate/surfcoat

Effect of particle size distribution of suspension feedstock on the microstructure and mechanical properties of suspension plasma spraying YSZ coatings

Pablo Carpio [a,*], Emilie Bannier [a], María Dolores Salvador [b], Amparo Borrell [b], Rodrigo Moreno [c], Enrique Sánchez [a]

[a] Instituto de Tecnología Cerámica (ITC), Asociación de Investigación de las Industrias Cerámicas (AICE), Universitat Jaume I (UJI), Av. Vicent Sos Baynat s/n, 12006 Castellón, Spain
[b] Instituto de Tecnología de Materiales (ITM), Universitat Politècnica de València (UPV), Camino de Vera s/n, 46022 Valencia, Spain
[c] Instituto de Cerámica y Vidrio (ICV), CSIC, c/Kelsen 5, 28049 Madrid, Spain

ARTICLE INFO

Available online 3 September 2014

Keywords:
Suspension plasma spraying
Yttria stabilised zirconia
Thermal barrier coating
Microstructure
Indentation

ABSTRACT

In this work, aqueous suspension feedstocks with different particle size distribution from submicron- and nano-sized YSZ powders were prepared. A previous colloidal characterisation allowed concentrated suspensions (~40 wt%) to be prepared. These suspensions were then successfully deposited by suspension plasma spraying (SPS) onto stainless steel substrates at different spraying distances. Coatings were characterised in terms of microstructure and mechanical properties (hardness and elastic modulus) by nanoindentation.
All coatings displayed a two-zone microstructure formed by partially melted areas containing nanometre or submicrometre-sized particles surrounded by fully melted areas. These partially melted areas strongly increased as standoff distance lengthened. Mechanical properties worsened with spraying distance increase. The finer the feedstock particle size the more the spraying distance effect was. A clear correlation between mechanical properties and amount of partially melted areas has been proved. Thus the use of a mixture of nano/submicron-sized particles as a SPS feedstock can represent a good balance between suspension processability and final coating performance.

1. Introduction

Previous research has shown that thermal barrier coatings (TBCs) obtained by suspension plasma spraying (SPS) exhibit enhanced properties when compared with conventional, APS (atmospheric plasma spraying) coatings [1–3]. Nevertheless the properties of the resulting coatings are very dependent on the feedstock suspension properties [4,5]. Hence the first step to produce good quality SPS coatings is to suitably disperse the particles into the liquid carrier to obtain stable suspensions which can be fed into the plasma torch through the injection system without clogging or settling [2,4]. Ethanol has been more extensively used as suspension solvent due to its lower vaporisation heat but water is preferable for sustainability reasons [6]. As reported elsewhere zeta potential represents the main indicator of the dispersion degree of a given suspension [7]. Therefore, the determination of this suspension characteristic and consequently the interpretation of colloidal interactions occurring in the suspension should be the first step when a concentrated, SPS feedstock is to be prepared. Although in principle higher solid content can be desirable in terms of deposition efficiency this content must be optimised to avoid clogging during injection as well as incomplete particle melting inside plasma torch.

With regard to particle size in the suspension feedstock, SPS technology ranges from few tens of nanometres to few microns. When nanoparticles are used, a much higher tendency to agglomerate is observed. Besides particle melting in plasma torch is also deeply affected by particle size distribution. Thus excessively small particles do not flatten so effectively meanwhile large particles and agglomerates have more tendency to remain partially unmelted [2].

Few attempts have been made to use feedstock mixtures of different particle size distributions, e.g. submicron/nano-sized particles despite their many potential advantages. The use of such bimodal distribution comprising the feedstock suspension can give rise to significant benefits during the suspension processing, i.e. higher solid content and lower viscosity leading to better feeding in the plasma torch along with higher deposition efficiency [4]. Besides some coating properties can be improved when using bimodal feedstock as recently reported for APS coatings [8,9]. However, the use of these bimodal powders has not been treated in SPS literature.

* Corresponding author at: Instituto de Tecnología Cerámica, Campus Universitario Riu Sec., Av. Sos Baynat s/n, 12006 Castellón, Spain. Tel.: +34 964342424; fax: +34 964342425.
E-mail addresses: pablo.carpio@itc.uji.es (P. Carpio), emilie.bannier@itc.uji.es (E. Bannier), dsalva@mcm.upv.es (M.D. Salvador), aborrell@upv.es (A. Borrell), rmoreno@icv.csic.es (R. Moreno), enrique.sanchez@itc.uji.es (E. Sánchez).

http://dx.doi.org/10.1016/j.surfcoat.2014.08.063
0257-8972/

Standard SPS process results in thinner coatings than those obtained by conventional APS process. As a consequence it has been successfully proven that nanoindentation technique is a more feasible method than conventional microindentation for mechanical characterisation of such layers. However, the amount of papers dealing with the use of nanoindentation method to characterise SPS layers is still very scarce [10]. In a recent work by some of the authors [11], it was proven that hardness and elastic modulus of SPS YSZ coatings could be estimated by this technique.

In the present study, concentrated and aqueous suspension feedstocks from commercial YSZ nanoparticles and submicron-sized particles were prepared and stabilised so as to obtain SPS coatings at different standoff distances. A previous colloidal characterisation of suspension feedstock in terms of zeta potential measurements was carried out. The coatings were microstructurally and mechanically characterised. The mechanical properties (elastic modulus and hardness) were determined by nanoindentation.

2. Experimental

2.1. Suspension preparation and characterisation

A commercial YSZ nanoparticle powder (5932HT, Nanostructured and Amorphous Materials Inc., USA), and a commercial YSZ submicron-sized powder (TZ-3YS, Tosoh Co., Japan) were used as raw materials. According to suppliers both powders contained 3 mol% yttria as well as tetragonal zirconia phase, the mean particle size was 40 nm and 400 nm for the nano- and submicron-sized powders respectively and the specific surface area was 25.1 and 6.8 m^2/g. In addition, the nanopowder also contained some small amount of monoclinic phase (not quantified). Furthermore, a commercial salt (DURAMAX™ D-3005, Rohm & Haas/Dow Chemicals, USA) of polyacrylic acid-based polyelectrolyte (PAA), with 35 wt% active matter was used as dispersant [12].

The colloidal stability of YSZ powders was assessed by zeta potential measurements (Zetasizer NanoZS, Malvern, UK) as a function of dispersant content and pH. In order to perform the measurements, diluted suspensions with 0.01 wt% YSZ and KCl 0.01 M as electrolyte were prepared. The pH values were determined with a pH-meter (Titrino DMS 716, Metrohm, Switzerland) and were adjusted with HCl and KOH solutions. A sonication probe (UP 400S, Dr Hielscher GmbH, Germany) was used in order to avoid agglomerations which can interfere in the analysis.

Concentrated suspensions from 100% nanoparticle and 100% submicron-sized particles with a solid content of 10 vol.% could then be prepared. The optimal amount of dispersant was used and different sonication times were employed. Subsequently a bimodal (50% nanopowder/50% submicron-sized powder) suspension with the same solid content was prepared following the procedure set out elsewhere [13]. The following references were used to name the suspension feedstocks: 100% nanoparticles (Yn), 100% submicron-sized particles (Ys) and 50% nano/50% submicron-sized powder (Ysn).

The rheological behaviour of some concentrated suspensions was determined using a rotational rheometer (Mars, Thermo Haake Co., Germany) operating at controlled shear rate (CR) by uploading the shear rate from 0 to 1000 s^{-1} in 300 s, maintaining at 1000 s^{-1} for 60 s and downloading from 1000 to 0 s^{-1} in 300 s. The measurements were carried out at 25 °C using a double-cone and plate system [13].

2.2. Coating deposition and characterisation

Coatings were deposited with a monocathode torch (F4-MB, Sulzer Metco, Switzerland) with a 6 mm internal diameter anode operated by a robot (IRB 1400, ABB, Switzerland). The substrates were preheated between 300 °C and 350 °C to enhance coating adhesion. The three suspensions (Yn, Ys and Ysn) were injected using a SPS system developed by the Instituto de Tecnología Cerámica (ITC). This system is formed by two pressurised containers which force the liquid to flow through a 150 μm diameter injector. A filter was used to remove agglomerates larger than 75 μm and possible contaminations. The following spraying parameters were kept constant from previous optimisation task: 37 slpm Ar, 8 slpm H_2, 700 A intensity, 1 m/s spraying velocity and 27 mL/min suspension feed rate (slpm: standard litre per minute). Three spraying distances were tested: 30 mm, 40 mm and 50 mm.

The coatings microstructure was analysed on polished cross-sections using a field-emission scanning electron microscope (S-4800, Hitachi Ltd., Japan). X-ray diffraction patterns were collected to identify crystalline phases in coating samples (Theta–Theta D8 Advance, Bruker, Germany). Coatings porosity as well as the amount of partially melted areas were estimated by image analysis at 5000× magnifications from SEM pictures following a procedure set out elsewhere [13]. Limitations of this technique to estimate very small (few hundreds of nanometres) pores were assumed [14]. Coating's hardness and elastic modulus were acquired by a nanoindenter (G-200, Agilent Technology, USA). Indentations were performed at 2000 nm constant depth using the Continuous Stiffness Measurement (CSM) method. A Berkovich diamond tip was used after the area function calibration procedure on fused silica was carried out assuring a tip radius below 100 nm. Average values of hardness and elastic modulus were then determined for a depth range from 100 to 200 nm. More details of this procedure can be found in previous research [10,11].

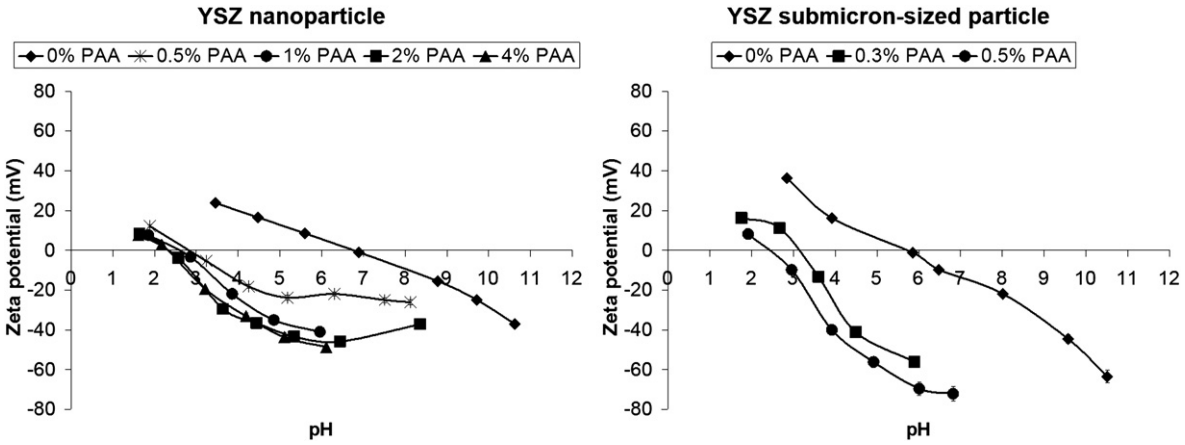

Fig. 1. Evolution of zeta potential of nano- and submicron-sized YSZ powders without dispersant and with different contents of PAA.

3. Results and discussion

Fig. 1 shows the evolution of zeta potential of nano- and submicron-sized YSZ powders without dispersant and with different contents of PAA. The isoelectric point (IEP) of these powders without additives occurs at 6.2 and 6.9 respectively, in good agreement with the values reported in the literature [12]. In both cases, IEP shifted to acid pH as the PAA content increased. This demonstrates that PAA was adsorbed on particle surface leading to well dispersed suspensions at working pH. Zeta potential curve does not change significantly for PAA contents >2 wt% in the case of nanoparticle suspension and >0.5 wt% in the case of submicron-sized suspension (not shown in the figure). It means that only these amounts of PAA were adsorbed on the particles. Consequently, the calculated amount of adsorbed dispersant (mass fraction of PAA adsorbed divided by particle specific surface area) in both cases was 0.8 mg/m^2 which agrees with previous reported data [7]. With this information concentrated aqueous suspensions of 10 vol.% (Yn, Ys and Ysn) were prepared which exhibited adequate rheological behaviour and stability so as to be injected into the plasma plume without sedimentation or clogging problems. The procedure to prepare these concentrated suspensions has been reported elsewhere [13].

From the prepared suspensions, coatings with 30 μm thickness were obtained. Fig. 2 shows the cross-sectional SEM images of the as-sprayed coatings obtained from Yn, Ys and Ysn feedstocks at the three spraying distances tested (in the case of the Yn sample the longest spraying distance was not realised). As reported elsewhere all the micrographs reveal *two-zones* microstructure, named as (*I*) melted and (*II*) sintered grain areas [11,15], which are displayed on the micrographs. For the sake of distinguishing porosity is also marked P in the micrographs. This microstructure develops because after the liquid is evaporated the resulting particles or agglomerates may thus be heated, partially melted, or fully melted, yielding the end coating. As a consequence the final microstructure largely depends on the characteristics of the suspension feedstock and plasma spraying conditions. As set out in the literature the heat flux significantly increases as the standoff distance diminishes giving rise to an enhanced cohesion and density in the coating [14–16]. As observed in Fig. 2, areas named *II* are clearly visible in all the coatings meanwhile the amount of these areas for a given feedstock seems to increase with the spraying distance. Fig. 3 plots the values of the amount of partially melted areas (*type II*) and porosity determined by SEM with the spraying distance. Overall high values of *type II* areas were obtained. Furthermore the evolution of the amount of these areas with spraying distance is quite evident. As spraying distance grows the amount of partially melted areas strongly increases. These high values of unmelted areas as well as the strong variation with spraying distance can be related to the fact that highly concentrated aqueous suspensions were used. Concentrated suspension feedstock requires high mass enthalpy to melt the particles meanwhile higher staking defect density within the layer is expected. This is particularly true when water is used instead of ethanol as solvent due to much higher enthalpy requirements of water [2,17].

Porosity data and their evolution with spraying distance are not so clear. On the one hand porosity values seem to be lower than those expected when compared with reported data obtained by other techniques [3,18]. This is probably due to the limitations associated to the assessment methodology by SEM, in particular for very small voids as mentioned earlier [14,18]. On the other hand the evolution of porosity data with spraying distance does not display a unique pattern. Hence porosity strongly increases when standoff distance rises for Yn and Ys feedstocks as expected by the evolution of the partially melted areas

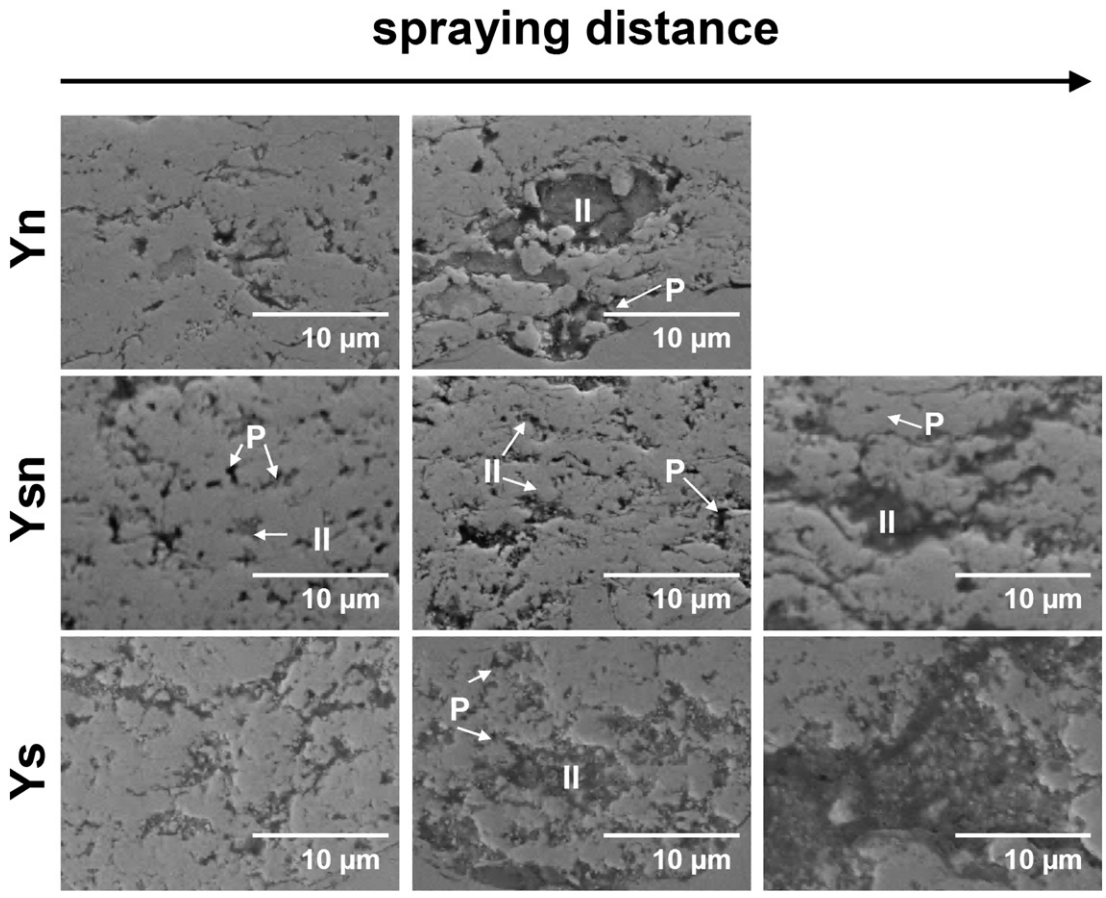

Fig. 2. Cross-sectional FEG-SEM images of the as-sprayed coatings obtained from Yn, Ys and Ysn feedstocks at the three spraying distances tested (only two for Yn feedstock). Voids (P) and *type II zones* (*II*) are marked.

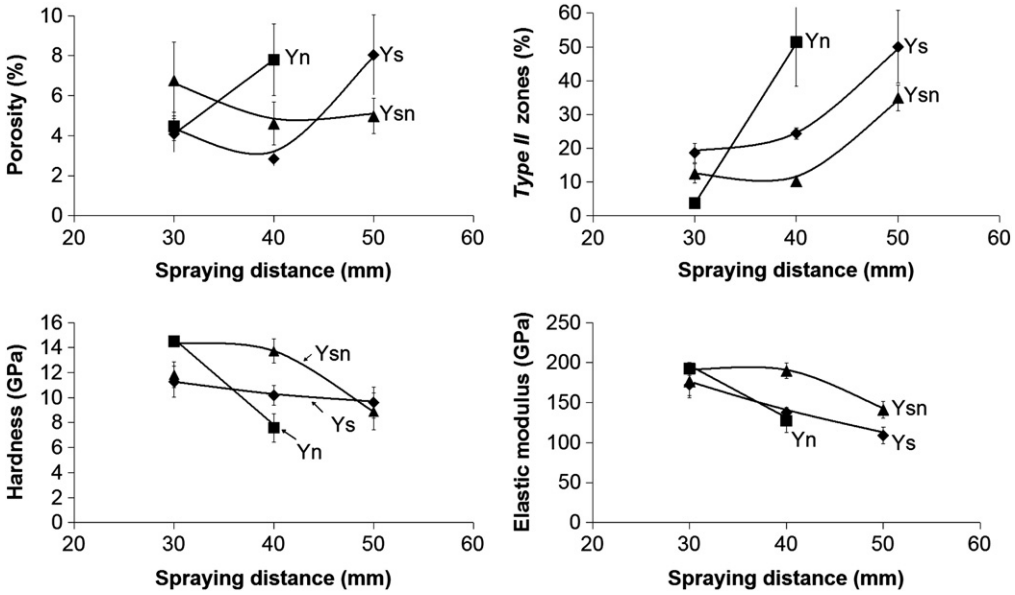

Fig. 3. Evolution of partially melted areas (*type II*), porosity, hardness and elastic modulus of the coatings with spraying distance.

set out above. However, the evolution of Ysn sample data does not follow this trend. This discrepancy is mainly based of an anomalous value of porosity for the 30 mm experiment probably due to the difficulty associated with the assessment of porosity in nanostructured layers. For this reason hereinafter the following discussions will be exclusively based on the amount of partially melted areas which show a much more reasonable evolution throughout the experiments carried out.

With regard to particle size of powder in the feedstock, a comparison of the amount of partially melted areas for the coatings at the three spraying distances reveal significant differences between samples. Although the effect of feedstock particle size in SPS process has been scarcely addressed, a recent review points out that the particle size distribution should be rather narrow as well as the agglomeration of small particles should be also avoided [2]. This is because excessively small particles (<500 nm) do not effectively flatten due to their lower inertia momentum and because they may re-solidify before impacting on the substrate. In this work the agglomeration of particles in the suspension feedstocks was avoided by efficient dispersing mechanism. Thus at the shortest spraying distance Yn coating exhibits the lowest amount of partially melted areas which dramatically increases as the spraying distance rises. Ys and Ysn feedstocks also display this behaviour but the variation with spraying distance is not so strong at least from 30 mm to 40 mm spraying distance. To try to explain the differences observed between nanoparticle feedstock (Yn) and the other two feedstocks (Ys and Ysn), Table 1 collects viscosity values of some suspensions obtained from the three powders. Viscosity data, taken from the downward flow curves at a shear rate of 1000 s^{-1}, were worked out from rheological measurements as set out earlier for Yn, Ys and Ysn suspensions at two solids concentration: 10 vol.% and 30 vol.%. As observed viscosity of a concentrated nanoparticle suspension is higher than that of suspensions containing submicron-sized particles due to stronger colloidal interactions [12]. These interactions and, consequently viscosity differences between nanoparticles and submicron-sized particles suspensions magnifies as the solid content increases. In this way, when the suspension jet is fed into the plasma plume and the water evaporation suddenly starts to occur the viscosity of fragmented nanoparticle suspensions strongly increases making it harder for the drying of fragmented droplet to progress. For this reason water removal becomes more difficult when the plasma enthalpy starts to decrease i.e. when the standoff distance increases. In these conditions, agglomeration of nanoparticles is very likely to occur regardless the initial stabilisation of the suspension feedstocks. This explanation agrees with the mechanism involved during the fragmentation and drying of droplets in SPS process [1,19]. Thus the melting of the outer part of the agglomerated nano/submicron-sized particles injected into the plasma plume together with the sintering of the inner nano/submicron-sized particles in these same agglomerates contribute to the partially melted zones development. This work highlights the role of suspension viscosity into this mechanism.

Table 1
Viscosity at 1000 s^{-1} shear rate of Yn, Ys and Ysn samples at two different solid content: 10 vol.% and 30 vol.%.

	Viscosity (mPa·s)	
	10 vol.%	30 vol.%
Yn	2.8	46.5
Ysn	2.0	17.9
Ys	1.8	13.3

On the other hand it is worthwhile mentioning that the evolution of the amount of *type II zones* with standoff distance for Ysn coating always runs below Ys sample's curve. However the viscosity of these two suspension is quite similar as a consequence of the particle packing efficiency of bimodal distribution (i.e. nano/submicron-sized) which results in lower viscosity values in comparison with nanoparticle suspension. This effect has already been reported in literature [20]. The effect of particle size is also significant since for similar suspension viscosity values, like Ys and Ysn suspension (see Table 1), the amount of *type II zones* for sample Ysn was always below Ys curve.

The complexity of the phenomena taking place during droplet formation and deposition in SPS process makes it necessary further research so as to assess the impact of suspension viscosity and solid particle size on the microstructure of the final deposited layers.

Finally XRD patterns of all coatings show the presence of tetragonal phase. This is the usual phase in as-sprayed coatings when the yttria proportion is 3 mol% [11]. However small peaks of monoclinic phase were detected in those coatings obtained from feedstocks containing nanoparticles due to the presence of monoclinic phase in the nanopowder as set out above. As example, Fig. 4 displays XRD pattern of coating obtained from Yn, Ysn and Ys suspensions at 40 mm.

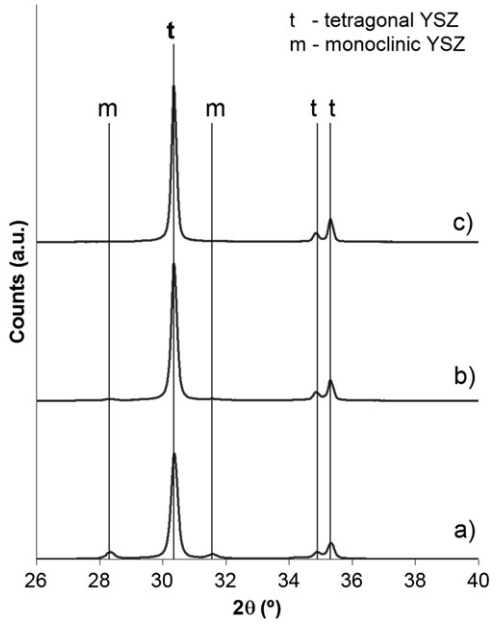

Fig. 4. XRD pattern of coatings obtained from Yn (a), Ysn (b) and Ys (c) suspensions at 40 mm standoff distance.

Fig. 3 shows the variations of the average values of hardness and elastic modulus obtained for each coating versus spraying distance. Firstly the magnitude of the obtained values agrees with previous reported data [11]. Overall for each coating, mechanical properties decrease when spraying distance increases. This variation clearly follows the inverse tendency undergone by the amount of *type II zones* in the coatings as can be deduced on comparing the corresponding plots in Fig. 3. As previously set out by the authors in YSZ SPS coatings [11] strong differences in mechanical properties were observed in the different microstructural zones (*type I* or *type II*) comprising the coatings. Unmelted or partially melted zones that are made up of partially sintered nanoparticles give rise to poor interparticle bonding. On the contrary, melted particles lead to stronger cohesion in the arrangement of nanoparticles improving the mechanical properties. Thus the presence of unmelted powders or partially melted particulates is desired to be minimised. In fact similar hardness and elastic modulus values to dense YSZ were obtained when amount of *type II zones* was low [21]. Secondly with regard to the effect of the feedstock particle sizes there is not a unique trend. At the shortest spraying distance, Yn feedstock gives rise to better mechanical properties which drastically worsen when increasing the spraying distance. Bearing in mind that particle or agglomerate size in SPS feedstock can be an order of magnitude smaller or more than that in APS, it can be understood that such as small agglomerates respond very rapidly to changes in plasma temperature and velocity [17] At the same time, as far as literature reports, the sprayability window is much narrower in liquid feedstock spraying [19]. This behaviour can be deduced on comparing the strong variation in mechanical properties for Yn feedstock with spraying distance with a much more gradual variation for Ys powder. Finally the feedstock comprising nano/submicron-sized particles undergoes a more robust evolution of mechanical properties against heat flux changes of plasma in this case provided by changes in spraying distance.

4. Conclusions

YSZ aqueous and concentrated suspensions from commercial nanoparticles and submicron-sized particles were successfully deposited by SPS at different standoff distances. Microstructure features by SEM and mechanical properties by nanoindentation were determined in all the coatings.

Stable (without sedimentation or aging) 10 vol.% suspensions of nanoparticles, submicron-sized particles and a mixture of nano/submicron-sized particles were prepared by using an adequate amount of dispersant which had been previously optimised by determining Z-potential curves. These three suspensions were used as feedstocks.

All coatings displayed a *two zones* microstructure with fully melted areas and sintered-grain areas where the nano- or submicrometre-structure was observed. Porosity and particularly partially melted areas significantly increased with spraying distance due to the reduction of heat flux. Except for the shortest spraying distance, at constant spraying distance partially melted areas strongly grew as the particle size content in the feedstock decreased (nanoparticle versus submicron-sized) due probably to the impact of suspension viscosity particle agglomeration when droplets dry.

Mechanical properties decreased as the spraying distance lengthened showing the inverse trend undergone by the amount of partially melted areas. Besides the coarser the particle size in the feedstock the more robust the variation of mechanical properties with standoff distance. In this way at intermediate or long spraying distances the coating obtained from the feedstock comprising nano- and submicron-sized particles displayed the best mechanical property values.

Thus the use of a mixture of nano/submicron-sized particles as a SPS feedstock can represent a good balance between suspension processability and final coating performance.

Acknowledgements

This work has been supported by the Spanish Ministry of Science and Innovation and by ERDF (European Regional Development Funds) (Project MAT2012-38364-C03). The authors also acknowledge the SCSIE of the University of Valencia for the FEG-SEM observations. Finally, the Research Promotion Plan of the Universitat Jaume I, action 3.1 (ref. PREDOC/2009/10) and the Spanish Ministry of Science and Innovation for Juan de la Cierva contract (JCI-2011-10498) is also grateful.

References

[1] L. Pawlowski, Surf. Coat. Technol. 203 (2009) 2807–2829.
[2] P. Fauchais, G. Montavon, R.S. Lima, B.R. Marple, J. Phys. D. Appl. Phys. 44 (2011) 093001.
[3] H. Kassner, R. Siegert, D. Hathiramani, R. Vassen, D. Stoever, J. Therm, Spray Technol. 17 (2008) 115–123.
[4] D. Waldbillig, O. Kesler, Surf. Coat. Technol. 203 (2009) 2098–2101.
[5] K. VanEvery, M.J.M. Krane, R.W. Trice, Surf. Coat. Technol. 206 (2012) 2464–2473.
[6] A. Moign, A. Vardelle, N.J. Themelis, J.G. Legoux, Surf. Coat. Technol. 205 (2010) 668–673.
[7] M. Vicent, E. Sánchez, I. Santacruz, R. Moreno, J. Eur. Ceram. Soc. 31 (2011) 1413–1419.
[8] M. Vicent, E. Bannier, R. Moreno, M.D. Salvador, E. Sánchez, J. Eur. Ceram. Soc. 33 (2013) 3313–3324.
[9] M.C. Bordes, M. Vicent, A. Moreno, R. Moreno, A. Borrell, M.D. Salvador, E. Sánchez, Surf. Coat. Technol. 220 (2013) 179–186.
[10] E. Rayón, V. Bonache, M.D. Salvador, E. Bannier, E. Sánchez, A. Denoirjean, H. Ageorges, Surf. Coat. Technol. 206 (2012) 2655–2660.
[11] P. Carpio, E. Rayón, L. Pawlowski, A. Cattini, R. Benavente, E. Bannier, M.D. Salvador, E. Sánchez, Surf. Coat. Technol. 220 (2013) 237–243.
[12] R. Benavente, M.D. Salvador, M.C. Alcazar, R. Moreno, Ceram. Int. 38 (2010) 2111–2117.
[13] T. Molina, M. Vicent, E. Sánchez, R. Moreno, Mater. Res. Bull. 47 (2012) 2469–2474.
[14] P. Fauchais, G. Montavon, J. Therm, Spray Technol. 19 (2010) 227–239.
[15] S. Kozerski, L. Łatka, L. Pawlowski, F. Cernuschi, F. Petit, C. Pierlot, H. Podlesak, J.P. Laval, J. Eur. Ceram. Soc. 31 (2011) 2089–2098.
[16] C. Delbos, J. Fazilleau, V. Rat, J.F. Coudert, P. Fauchais, B. Pateyron, Plasma Chem. Plasma Process. 26 (2006) 393–414.
[17] O. Tingaud, P. Bertrand, G. Bertrand, Surf. Coat. Technol. 205 (2010) 1004–1008.
[18] A. Bacciochini, G. Montavon, J. Iiavsky, A. Denoirjean, P. Fuchais, J. Therm, Spray Technol. 19 (2010) 198–206.
[19] P. Fauchais, R. Etchart-Salas, V. Rat, J.F. Coudert, N. Caron, K. Wittmann-Ténèze, J. Therm, Spray Technol. 17 (2008) 31–59.
[20] M. Vicent, E. Sánchez, T. Molina, M.I. Nieto, R. Moreno, Ceram. Int. 39 (2013) 9091–9097.
[21] L. Latka, D. Chicot, A. Cattini, L. Pawlowski, A. Ambroziak, Surf. Coat. Technol. 220 (2013) 131–139.